# Progressive crushing 40Ar/39Ar dating of gold-bearing quartz vein from the Liaotun Carlin-type gold deposit at the northwest of Guangxi

**Rongguo Hu**
College of Earth Sciences and Guangxi Key Laboratory of Hidden Metallic Ore Deposits Exploration, Guilin University of Technology

**Baocheng Pang** ( pbc@glut.edu.cn )
College of Earth Sciences and Guangxi Key Laboratory of Hidden Metallic Ore Deposits Exploration, Guilin University of Technology

**Xiujuan Bai**
Key Laboratory of Tectonics and Petroleum Resources of Ministry of Education, China University of Geosciences (Wuhan)

**Lingan Bai**
College of Earth Sciences and Guangxi Key Laboratory of Hidden Metallic Ore Deposits Exploration, Guilin University of Technology

**Xijun Liu**
College of Earth Sciences and Guangxi Key Laboratory of Hidden Metallic Ore Deposits Exploration, Guilin University of Technology

**Yuanqiang Li**
College of Earth Sciences and Guangxi Key Laboratory of Hidden Metallic Ore Deposits Exploration, Guilin University of Technology

**Jianqi Xu**
College of Earth Sciences and Guangxi Key Laboratory of Hidden Metallic Ore Deposits Exploration, Guilin University of Technology

**Huaning Qiu**
Key Laboratory of Tectonics and Petroleum Resources of Ministry of Education, China University of Geosciences (Wuhan)

**Research Article**

**Keywords:**

**Posted Date:** March 15th, 2022

**DOI:** https://doi.org/10.21203/rs.3.rs-1418453/v1

## Abstract

Progressive crushing $^{40}Ar/^{39}Ar$ dating has been performed on a gold-bearing quartz vein from the Liaotun Carlin-type gold deposit at the northwest of Guangxi for the first time. Gases liberated from the secondary and primary fluid inclusions yielded two age plateau with ages of 168.4 ± 1.9 Ma and 200.5 ± 1.9 Ma, respectively. The data points constituting the age plateau yielded excellent inverse isochrons with isochron ages of 167.0 ± 1.9 Ma and 200.7 ± 2.1 Ma. The initial $^{40}Ar/^{36}Ar$ ratios corresponding to the two isochrons are 308.9 ± 6.8 and 298.0 ± 4.3, which are statistically indistinguishable from the air, indicating that the ore-forming fluids probably mainly derived from the basin pressure flow dominated by atmospheric precipitation. The age from the PFIs of 200.5 ± 1.9 Ma can be taken as the timing of Au mineralization. In contrast, the age of 167.0 ± 1.9 Ma recorded by SFIs represents the timing of late hydrothermal fluid superposition and transformation after the formation of gold deposit. Our preliminary study shows the feasibility and great potential of $^{40}Ar/^{39}Ar$ dating by progressive crushing of fluid inclusions from quartz vein to date the mineralization age and decipher the fluid origins of Carlin-type gold deposits.


## Introduction

The Yunnan(Dian)-Guizhou(Qian)-Guangxi(Gui)-area of southwestern China is well known as the “Golden Triangle” since this region contains the second-largest concentration of Carlin-type gold deposits in the world (Fig. 1a, b), with a total resource of > 800 tons of contained Au at Au an average grade of 4.5 g/t[1–10]. Precise geochronological data of mineralization within micro-fine disseminated rocks, such as the Carlin-type/like gold deposits are not always available, since they are generally lack datable minerals for conventional isotopic dating techniques[5,11–14]. However, with the progress of mineral separation and isotopically analytical technologies, as well as the development and utilization of new techniques, great progress has been made in constraint the metallogenic ages of Carlin-type gold deposits during the past decades[4,14,15]. For example, the metallogenic ages of Carlin-type gold deposits in Nevada, USA, have been well constraint on 42 – 36 Ma by applied Rb-Sr and $^{40}Ar/^{39}Ar$ dating methods of galkhaite and adularia, respectively[11,16,17].

There is no galkhaite and adularia in Carlin-type gold deposits from the Dian-Qian-Gui area “Golden Triangle” have been reported, thus, the published isotopic dating results from this region (Fig. 1b) mainly derived from hydrothermal altered minerals and fluid inclusions Rb-Sr dating[19–21,28], arsenopyrite, pyrite and pyrobitumen Re-Os dating[6,8,22], hydrothermal rutile/monazite/calcite/apatite U-(Th)-Pb method[4,9,15,23], zircon U-Th-He method[29], sericite and illite $^{40}Ar/^{39}Ar$ dating[27], and hydrothermal calcite Sm-Nd method[24–26]. In summary, the reported geochronological data suggested that the Dian-Qian-Gui “Golden Triangle” region underwent two independent gold mineralization events during the late Triassic to early Jurassic (230 ~ 195 Ma) and the late Jurassic to early Cretaceous (150 ~ 122 Ma).

As one of the typical Carlin-type gold deposit in Bama County, northwest Guangxi (Fig. 1c), precise mineralization age of the Liaotun gold deposit is still poorly constrained mainly because no suitable minerals can be selected for traditional isotopic dating methods. Gold deposit in the district is hosted by middle Permian Baifeng Formation ($T_2bf$) that consists of mudstone, sandstone and siltstone, and the orebodies are mainly controlled by NW-trending or EW-trending faults (Fig. 1c). A felsic dike intruded Carboniferous limestone and Triassic sandstone along an ENE- to NE-trending fault and cut off the biggest orebody (No. I). The $^{40}Ar/^{39}Ar$ dating of muscovite phenocryst from this dike yielded a plateau age of 95.5 ± 0.7 Ma, which is interpreted as the upper limit of the metallogenic epoch[18]. Later, SIMS zircon U-Pb dating result shows that the Liaotun dike was emplaced at 97.2 ± 1.1 Ma (MSWD = 2.9), and the authors inferred that there is no genetic link between the felsic dike and Liaotun carlin-type gold deposit[30]. Therefore, in order to unravel the precise mineralization age of this gold deposit, there still needs more accurate direct metallogenic data.

The $^{40}Ar/^{39}Ar$ *in vacuo* progressive crushing technique for dating the ages of fluid inclusions has been improved and developed for thirty-five years[31]. This method has been widely applied to constrain the formation ages of hydrocarbon accumulation[32,33], high-ultrahigh pressure retrograde metamorphism[34,35], and especial on direct dating of hydrothermal deposit minerals (Cassiterite, sphalerite, wolframite) and gangue minerals like mineralization quartz vein[36–43]. Nevertheless, there is still no successful report by

this technique on sediment-hosted Carlin-type gold deposits yet, although mineralization quartz veins with abundant fluid inclusions are widely developing in this type of ore deposit.

In this contribution, we chose the Liaotun Carlin-type gold deposit, northwest Guangxi, as the research object, applying the $^{40}Ar/^{39}Ar$ *in vacuo* progressive crushing dating technique on the main mineralization stage pyritized gold-bearing quartz vein for the first time (Fig. 2c). Based on a combined approach of fluid inclusions petrographic observation and micro-thermometric measurement, our study is try to decipher the origin of fluid flow and constrain the age of quartz vein formation by using a direct approach. Furthermore, we believe our attempt not only can evaluate the feasibility of $^{40}Ar/^{39}Ar$ dating by *in vacuo* progressive crushing of fluid inclusions, but also could exploit a new approach to constraint the mineralization age of the lack datable minerals Carlin-type/like gold deposits.

# Geological setting

The Dian-Qian-Gui ore concentration area is restricted to the Devonian-Triassic Youjiang basin, which is bound to the northeast by the Ziyun-Du'an fault, to the northwest by the Mile-Shizong fault, and to the southeast by the Pingxiang fault (Fig. 1b), which separates the basin from the Cathaysia block[1]. It widely developed Au-As-Sb-Hg low-temperature hydrothermal deposits and contains one of the largest concentrations of Carlin-type gold deposits in the world[1–3,8,10].

Evolution of the Youjiang Basin can be divided into six stages from Early Devonian to Cretaceous[44], while gold deposits in this region mainly formed in the tectonic transformation period from Indosinian compression Orogeny to Yanshanian extensional tectonic environment, that is, the extension stage after the collision of Youjiang fold belt formed by the evolution of foreland basin in Youjiang Basin[1,2,4,6,44]. All gold deposits over the Golden Triangle are mainly hosted in the Permian limestone and volcaniclastic sedimentary rocks or Triassic siliciclastic rocks and carbonates and are structurally controlled by various folds and associated faults, likely produced during the Indosinian orogenic deformation[1,45].

# Geology of the Liaotun Deposits

The fault type Liaotun gold deposit, in Bama County, Northwest Guangxi, is a medium-sized Carlin-type gold deposit, which located on southwest margin of the isolated Longtian carbonate platform (Fig. 1b)[18,30,46]. The exposed sedimentary rocks in the platform are mainly limestone intercalated with dolomite of Carboniferous Du'an Formation ($C_{1-2}d$) and Permian sponge reef limestone (P*bls*). The strata around the platform is the Triassic Baifeng Formation ($T_2bf$), which consists of interbedded deep-water basin facies sandstone and mudstone (Fig. 2a)[18,30].

The study area contains well-developed faults and linear folds and individual gold orebodies are structurally controlled by high-angle faults. There are five NW-trending and four EW-trending faults have been recognized in the mine area (Fig. 1c). Among them, the NW-trending faults F1 and F2 are syn-sedimentary faults, while the NW-trending F4 and the EW-trending F5, F6, F9 faults are ore-controlling/bearing structures, hosting the I, III, IV, and V orebodies, respectively (Fig. 1c)[18,46]. A later Yanshanian (97 – 95 Ma) quartz porphyry veins intruded Carboniferous limestone and Triassic sandstone along an ENE- to NE-trending fault across the Longtian dome[18,30].

The deposit consists of five orebodies and the largest orebody (No. I) is cut off by the later Yanshanian quartz porphyry vein from the middle and respectively named as I-1 and I-2 (Fig. 1c). Gold mineralization occurred in shallow part is oxidized ore, dominant by silicification and limonitization detrital quartz greywacke and cataclasite. Primary to semi-primary ore minerals in deeper part are disseminated pyrite and minor Arsenopyrite. Hydrothermal alterations associated with gold mineralization in the deposit have identified silicification, pyritization, arsenopyrite, (de)carbonatination, clayization and sulfidation. In additionally, the occurrence, textures, and mineral assemblages of the ores at Liaotun indicate that the main-mineralization stages can be further divided into: (1) decarbonination + silicification stage; (2) quartz + pyrite + arsenopyrite stage; (3) quartz + stibnite stage; (4) quartz + calcite + clayization stage[18,46].

The NW-trending F4-controlling largest I orebody is 656 m long and average 9 m thick, with steep dip angles of 50° to 85° and an average grade of 1.62 g/t Au. The smaller III and V orebodies are controlled by EW-trending vertical F5 and F6, which are 230 to 194 m long and 7.20 to 1.16 m thick with average gold grades varying from7.33 to 0.34 g/t Au[18,46]. The V orebody is hosted in siltstone, mudstone and thick bedded sandstone at the second member of middle Triassic Baifeng Formation. In this orebody, the dominant ore are taupe and purplish red silicified fine-sandstone, cataclasite, crushed rock, minor silicified siltstone and bedded mud, and veinlet quartz usually can be observed locally (Fig. 1c). The ore structures are disseminated, spotted, micro-veined-network, brecciated, porous and earthy[18]. The sample LT19-1-2 used in this study for fluid inclusion *in vacuo* crushing $^{40}Ar/^{39}Ar$ dating was collected from the goaf of V orebody (Fig. 2b, c). It is a 0.5-2 cm wide pyritized gold-bearing quartz vein with grade of 4.02 g/t Au[46].

## Results

# Fluid inclusion analyses

Petrographic observation and micro-thermometric measurements have been applied to the gold-bearing vein quartz samples from the Liaotun Carlin-type gold deposit. The total salinities ($W$) are calculated with the reduction formula based on the final ice-melting temperatures ($|T_m|$)[47]: $W = 1.78|T_m| - 0.0442|T_m|^2 + 0.000557|T_m|^3$. Two or three single fluid inclusions in each cluster were selected for measurement.

Abundant fluid inclusions developed in the quartz and can be separated into primary (PFIs) and secondary (SFIs) inclusions based on the textural criteria. Most of the PFIs are generally less than > 5 μm in diameter and characterized by two-phase (liquid-vapor) with an extremely small $CO_2$ bubble at room temperature (Fig. 3a). They normally have negative crystal, round, elongate, or irregular shapes, and observed as isolated, random or clustered distributions (Fig. 3b, c), suggesting a primary origin. Heating-freezing stage analysis shows that the type-b inclusions have $T_m$ between − 6.5 and − 9.5°C, corresponding to salinities of 9.9–13.4 wt.% NaCl equivalent. The homogenization temperature is between 245 and 180°C. The tiny linear distributions SFIs (~ 1–3 μm in size) are mainly occurring along cross-cutting healed fractures and have round, oval, tubular or irregular shapes (Fig. 3a, d, e), but some irregular SFIs can reach 5–10μm. These inclusions are commonly pure aqueous inclusions, but two-phase ($CO_2$ + $H_2O$) inclusions have been observed occasionally. The measured results gave $T_m$ values between − 2.1 and − 7.5°C, corresponding to salinities of 3.5–11.1 wt.% NaCl equivalent. Values for $T_h$ were measured between 200 and 160°C.

### $^{40}$ Ar/ $^{39}$ Ar Dating Result

During *in vacuo* crushing experiment, quartz separates LT19-1-2Qz underwent 33 stages and around 16990 number of stokes. The age spectra for this sample, shown in Fig. 4, yield a monotonically decreasing staircase-shaped age spectrum with apparent ages from 268 to 191 Ma in the first four stages. Subsequently, upon continued crushing, the apparent ages from steps 5 to 11 gradually stabilize to reveal age plateaux, with plateau age of 168.4 ± 1.9 Ma (Fig. 4a, $^{39}$Ar = 42%, MSWD = 5.5) and K/Ca ratios of 11.6 ± 3.7(Fig. 4b). The data points of these steps defining the plateau age yields isochron with age of 167.0 ± 1.9 Ma (MSWD = 2.3), corresponding to an initial $^{40}Ar/^{36}Ar$ ratio of 308.9 ± 6.8 (Fig. 4c). Apparent ages rise from 175.7 Ma at step 12 to 191.5 Ma at step 15 and then followed by a flat plateau by steps 16 to 33, with plateau age of 200.5 ± 1.9 Ma (Fig. 4a, $^{39}$Ar = 24%, MSWD = 0.6) and K/Ca ratios of 4.1 ± 1.0 (Fig. 4b). On the inverse isochron diagram of $^{36}Ar/^{40}Ar$ vs. $^{39}Ar/^{40}Ar$, these data points define an excellent linear array, and yield an age of 200.7 ± 2. Ma (MSWD = 1.6) with an initial $^{40}Ar/^{36}Ar$ ratio of 298.0 ± 4.3, which are consistent with the plateau age as well as the atmospheric value for the $^{40}Ar/^{36}Ar$ ratio (Fig. 4c).

## Discussions

**Age significances of $^{40}Ar/^{39}Ar$ crushing dating.** Fluid inclusions in mineral-hosted analysis is one of the most important techniques in modern studies of hydrothermal mineral deposits, as the trapped fossil fluids inclusions could directly provide pivotal information on the geochemistry and geochronology of mineralization systems[48–51]. The key point and the most difficulties of fluid inclusions geochronological study is how to effectively distinguish and extract the gases from the SFs and PFs

respectively[31,37–39,41,52,53]. Just as described by Bodnar[54], "PFIs are formed during, and as a direct result of, growth of the surrounding host crystal. If a crystal fractures after it has been formed, some fluid may enter the fracture and become trapped as SFIs as the fracture heals. Thus, SFIs are trapped after crystal growth is complete". As a result, the SFIs and PFIs are generally yield different in volume and have distinctive distribution characteristics. Generally, in the process gas-extraction by *in vacuo* crushing method, SFIs are easily crushed and liberated gases at the initial steps, while the PFs can be extracted in the later crushing steps[31,39,55]. Part of the bigger PFIs which occur along the healed micro-cracks are probably also extracted during the earlier steps. Additionally, experiments show that as long as the crushing times are enough, gases from most of the > 1 μm fluid inclusions can be extracted effectively[38,41].

In the case of sample LT19-1-2Q, SFIs are crushed and liberated gases at the initial steps yields inverse isochron age of 167.0 ± 1.9 Ma (Fig. 4c). This age represents an episode of late hydrothermal fluid superposition and transformation after the formation of gold deposit. Published isotopic ages indicating the metallogenic ages of the Carlin-type gold deposits in the north of "Golden Triangle" are mainly concentrated at 150 – 130 Ma[1–4,24], while the magmatic activities in this region are concentrated at 96 – 77 Ma[18,30,56]. Thereby, this age whether represents another period of mineralization still need to be further studied. With crushing continues, the SFIs were gradually exhausted whereas PFs dominate the gas contribution and yield an isochron age of 200.5 ± 1.9 Ma (Fig. 4c). Since the pyritized gold-bearing quartz vein in Liaotun is the main-metallogenic stage production and its Au grade as high as ca. 4 g/t, the age of PFs then can be taken as the best estimate for the timing of Au mineralization, which is basically coeval with the metallogenic age of the main Carlin-type gold deposits in the central and southern part of Youjiang ore concentration area of South China[1,2,4]. Combined with previous studies, we suggest that the Liaotun gold deposit formed in the tectonic transformation period from Indosinian compression Orogeny to Yanshanian extensional tectonic environment, that is, the extension stage after the collision of Youjiang fold belt formed by the evolution of foreland basin in Youjiang Basin.

**Fluids origin and evolution constraints.** Reported noble gas (He, Ne, Ar) isotope data of fluid inclusions extracted from arsenian pyrite, quartz, calcite and fluorite from Shuiyindong, Nibao and Yata Carlin-type gold deposits indicate that the main ore-stage fluids are a mixture of ascending magmatic fluid and sedimentary pore fluid, whereas the late ore-stage fluids are a mixture of sedimentary pore fluid or deeply sourced metamorphic fluid and shallow meteoric groundwater[1,3,20,45]. On the other hand, *In situ* SIMS analysis on Au-bearing pyrites from the Jinya, a Carlin-type gold deposit close to Liaotun (Fig. 1c), yields similar $\delta^{34}S$ values (ca. − 6.22‰) with the surrounding sedimentary basin (ca. − 7‰), suggesting that the fluids that formed the deposit may meteoric waters transported by regional faults derived from the surrounding sedimentary basin[57].

The initial $^{40}Ar/^{36}Ar$ ratio of fluid inclusions provides information on fluid origins[40,42]. Previous studies have demonstrated the deep magmatic metallogenic hydrothermal fluids, especially mantle derived hydrothermal fluids, generally contain excess $^{40}Ar$[39,40,42,43,53]. In terms of *in vacuo* progressive $^{40}Ar/^{39}Ar$ dating of fluid inclusions from this study, as shown in Fig. 4c, the initial values of $^{40}Ar/^{36}Ar$ of SFIs and PFIs in gold bearing quartz vein are 308.9 ± 6.8 and 298.0 ± 4.3, respectively, which are consistent with the modern atmospheric $^{40}Ar/^{36}Ar$ ratio, indicating that there is basically no excess $^{40}Ar$ in either SFIs or PFIs. Therefore, we prefer to consider the ore-forming fluids of the Liaotun gold deposit is mainly derived from meteoric waters transported by regional ore-controlling faults and/or basinal fluids derived by gravitational pressure.

The Ar-isotopic compositions trapped in fluid inclusions also carries a signature of source of the fluid and the processes which have affected them [34,39,40,42,55,58]. As shown in Fig. 5, the SFIs have higher $^{39}Ar_K$, $^{38}Ar_{Cl}$ and $^{37}Ar_{Ca}$ signals, reflecting relatively higher potassium and chlorine contents dissolved in the SFI fluid. This fact may indicate that the SFIs had a strong water-rock reaction with the country rocks resulting in much potassium dissolved. This is consistent with the ore deposit occurs in rich potassium-bearing minerals (mica/sericite and K-feldspar) Triassic siltstone and mudstone. In other words, the SFIs may derive from the regional faults transported meteoric waters and the high potassium in the SFIs is probably correlated with $Cl^-$ and/or $HCl^-$ dissolved in the fluids. It should be noted that the PFIs have higher signals of $^{37}Ar_{Ca}$ than $^{38}Ar_{Cl}$ and relatively lower K/Ca ratio (Fig. 4b and Fig. 5). This fact may imply that the ore-forming hydrothermal fluids should have intensive water-rock reaction with calcium-rich rather than potassium-rick rocks, and the potassium in the PFIs is probably correlated with $HCO_3^-$ and $CO_2^-$ dissolved in the ore-forming fluid[39]. In other words, the origin of the PFIs more likely gravitational pressure derived basinal fluids, which was once mainly carried and migrated by carbonate or/and dolomite rocks within the sedimentary basin.

# Methods

Fluid inclusions heating and freezing measurements were performed on doubly polished thick sections of the gold-bearing quartz vein by using a Linkam THMS 600 freezing/heating stage coupled to a BX51 Olympus polarizing microscope, at Guilin University of Technology. The rate of heating and cooling are normally ~ 10°C/min and reduced to 2°C/min near phase changes. The homogenization temperatures ($T_h$) of aqueous fluid inclusions that homogenize to the liquid phase and the temperatures of ice-melting ($T_m$) were measured. Homogenization temperatures are the minimum trapping temperatures, whereas ice-melting temperatures provide a measure of the fluid salinity[47].

The sample was crushed with the jaw crusher and sieved to obtain a size fraction of 500–1000 μm, and then put in $HNO_3$ to dissolve the carbonate fraction. Finally, all the samples were hand-picked under the binocular microscope. Samples were wrapped in aluminium foil and loaded into aluminium vessels together with standards and irradiated at the China Mianyang Research Reactor. Irradiation times were 40 hrs for irradiation WH01. As flux monitor standards for *J*-value calculation for this project were using ZBH-2506 with an assumed age of 132.7 ± 0.5 Ma, which was carried out in the Australian National University[59]. The monitor standard was inserted between every two to four samples, for irradiation *J*-value calculation. *In vacuo* crushing experiments were carried out in an in-house designed crushing apparatus which was connected to a three stage extraction line and connected with an ARGUS VI® noble gas mass spectrometer in MOE key Laboratory of Tectonics and Petroleum Resources, China University of Geosciences (Wuhan). The gases released were purified by a Zr/Al getter pump operated at room temperature and another Zr/Al pump operated at 400°C for 400 seconds. Mass discrimination (0.99745–0.99749 per atomic mass unit) was monitored by frequent analysis of $^{40}Ar/^{38}Ar$ reference gas pipette aliquots. Correction factors for interfering argon isotopes derived from Ca and K isotopes are: $(^{39}Ar/^{37}Ar)_{Ca}$ = 0.0006175, $(^{36}Ar/^{37}Ar)_{Ca}$ = 0.002348, $(^{40}Ar/^{39}Ar)_{K}$ = 0.002323 and $(^{38}Ar/^{39}Ar)_{K}$ = 0.009419. The $^{40}Ar/^{39}Ar$ data were calculated and plotted using the ArArCALC software package of[60]. Detailed data and relevant parameters for $^{40}Ar/^{39}Ar$ progressive crushing experiments are listed in Supplementary Table S1. Age spectrum and inverse isochron of the sample is illustrated in Fig. 4. Both the plateau and inverse isochron age uncertainties are given at the 2σ level.

# Declarations

Data availability

All the data are reported in the Supplementary Information.

Acknowledgments

We sincerely thank Dr. Zhipeng Xia and Mr. Guofeng Zheng for their kind help in thin section preparation and technical support for fluid inclusions analyses. This work was funded by the Natural Science Foundation of China (41362006; 41873017) and the Guangxi Natural Science Foundation Program (2020GXNSFAA297049).

Author Contributions

R.G.H defined the research theme, interpreted the results and wrote the paper. B.C.P revised the manuscript and provided financial support. X.J.B and H.N.Q helped to Ar-Ar dating and reviewed the manuscript. The other authors helped to collect and pretreat the samples, prepared Figure 1-3 and reviewed the manuscript. All authors reviewed the manuscript.

Competing Interests

The authors declare no competing interests.

Additional Information

**Correspondence** and requests for materials should be addressed to B.C.P. or R.G.H.

# References

1. Su, W. C. *et al.* Carlin-Type Gold Deposits in the Dian-Qian-Gui “Golden Triangle” of Southwest China. *Rev. in Econ. Geol.* **20**, 157-185 (2018).
2. Hu, R. Z. *et al.* The giant South China Mesozoic low-temperature metallogenic domain: Reviews and a new geodynamic model. *J Asian Earth Sci.* **137**, 9-34 (2017).
3. Su, W. C. *et al.* Sediment-Hosted Gold Deposits in Guizhou, China: Products of Wall-Rock Sulfidation by Deep Crustal Fluids. *Econ Geol.* **104**, 73-93 (2009).
4. Jin, X. Y. *et al.* Calcite U-Pb dating unravels the age and hydrothermal history of the giant shuiyindong carlin-type gold deposit in the golden triangle, south china. *Econ Geol.* **116**, 1253-1265 (2021).
5. Hu, R. Z., Su, W. C., Bi, X. W., Tu, G. Z. & Hofstra, A. H. Geology and geochemistry of Carlin-type gold deposits in China. *Miner Deposita.* **37**, 378-392 (2002).
6. Chen, M. H., Mao, J. W., Li, C., Zhang, Z. Q. & Dang, Y. Re–Os isochron ages for arsenopyrite from Carlin-like gold deposits in the Yunnan–Guizhou–Guangxi “golden triangle”, southwestern China. *Ore Geol Rev.* **64**, 316-327 (2015).
7. Lin, S. R. *et al.* An in situ sulfur isotopic investigation of the origin of Carlin-type gold deposits in Youjiang Basin, southwest China. *Ore Geol Rev.* **134**, 104187 (2021).
8. Ge, X. *et al.* Genetic relationship between hydrocarbon system evolution and Carlin-type gold mineralization: Insights from Re-Os pyrobitumen and pyrite geochronology in the Nanpanjiang Basin, South China. *Chem. Geol.* **559**, 119953 (2021).
9. Gao, W. *et al.* U-Pb Dating on Hydrothermal Rutile and Monazite from the Badu Gold Deposit Supports an Early Cretaceous Age for Carlin-Type Gold Mineralization in the Youjiang Basin, Southwestern China. *Econ Geol.* **116**, 1355-1385 (2021).
10. Peters, S. G., Jiazhan, H., Zhiping, L. & Chenggui, J. Sedimentary rock-hosted Au deposits of the Dian–Qian–Gui area, Guizhou, and Yunnan Provinces, and Guangxi District, China. *Ore Geol Rev.* **31**, 170-204 (2007).
11. Groff, J. A., Heizler, M. T., McIntosh, W. C. & Norman, D. I. $^{40}Ar/^{39}Ar$ dating and mineral paragenesis for carlin-type gold deposits along the Getchell Trend, Nevada; evidence for Cretaceous and Tertiary gold mineralization. *Econ Geol.* **92**, 601-622 (1997).
12. Cline, J. S. Timing of Gold and Arsenic Sulfide Mineral Deposition at the Getchell Carlin-Type Gold Deposit, North-Central Nevada. *Econ Geol.* **96**, 75-89 (2001).
13. Arehart, G. B. Characteristics and origin of sediment-hosted disseminated gold deposits: a review. *Ore Geol Rev.* **11**, 383-403 (1996).
14. Arehart, G. B. *et al.* Evaluation of Radioisotope Dating of Carlin-Type Deposits in the Great Basin, Western North America, and Implications for Deposit Genesis. *Econ Geol.* **98**, 235-248 (2003).
15. Chen, M. H., Bagas, L., Liao, X., Zhang, Z. Q. & Li, Q. L. Hydrothermal apatite SIMS Th-Pb dating: Constraints on the timing of low-temperature hydrothermal Au deposits in Nibao, SW China. *Lithos.* **324-325**, 418-428 (2019).
16. Tretbar, D. R., Arehart, G. B. & Christensen, J. N. Dating gold deposition in a Carlin-type gold deposit using Rb/Sr methods on the mineral galkhaite. *Geology.* **28**, 947-950 (2000).
17. Hofstra, A. H. & Cline, J. S. Characteristics and Models for Carlin-Type Gold Deposits. *Rev. in Econ. Geol.* **13**, 163-220 (2000).
18. Chen, M. H., Mao, J. W., Wu, L. L. & Zheng, J. M. Determination of upper limit of metal logenic epoch of Liaotun gold deposit in western Guangxi and its implications for chronology of Carlin-type gold deposits in Yunnan-Guizhou-Guangxi "golden triangle" area. *Miner Depos.* **33**, 1-13 (2014).
19. Jin, X. Y. Geology, mineralization and genesis of the Nibao, Shuiyindong and Yata gold deposits in SW Guizhou Province, China. *China University of Geosciences (Wuhan)* (2017).
20. Liu, P. *et al.* A gold deposit associated with pyroclastic rock and hydrothermal exhalation: Nibao gold deposit in Guizhou province, China. *Miner Depos.* **25**, 101–110 (2006).
21. Zheng, L. L., Yang, R. D., Gao, J. B., Chen, J. & Li, D. P. Quartz Rb-Sr Isochron Ages of Two Type Orebodies from the Nibao Carlin-Type Gold Deposit, Guizhou, China. *Minerals.* **9**, 399 (2019).
22. Chen, M. H. *et al.* Re-Os dating of arsenian pyrites from the Lannigou gold deposit, Zhenfeng, Guizhou province, and its geological significances. *Geol Rev.* **53**, 371–382 (2007).

23. Pi, Q. H., Hu, R. Z., Xiong, B., Li, Q. L. & Zhong, R. C. In situ SIMS U-Pb dating of hydrothermal rutile: reliable age for the Zhesang Carlin-type gold deposit in the golden triangle region, SW China. *Miner Deposita*. **52**, 1179-1190 (2017).
24. Su, W. C., Hu, R. Z., Xia, B., Xia, Y. & Liu, Y. P. Calcite Sm-Nd isochron age of the Shuiyindong Carlin-type gold deposit, Guizhou, China. *Chem. Geol.* **258**, 269-274 (2009).
25. Tan, Q. P. *et al.* Two Hydrothermal Events at the Shuiyindong Carlin-Type Gold Deposit in Southwestern China: Insight from Sm–Nd Dating of Fluorite and Calcite. *Minerals*. **9**, 230 (2019).
26. Wang, Z. Genesis and dynamic mechanism of the epithermal ore deposits, SW Guizhou, China—a case study of gold and antimony deposits. *Institute of Geochemistry, Chinese Academy of Sciences*, 1-150 (2013).
27. Chen, M. H., Huang, Q. W., Hu, Y., Chen, Z. Y. & Zhang, W. Genetic types of phyllosilicate (Micas) and its $^{39}$Ar-$^{40}$Ar dating in Lannigou gold deposit, Guizhou province, China. *Acta Mineral Sin*. **29**, 353-362 (2009).
28. Hu, R. Z., Su, W. C., Bi, X. W. & Li, Z. Q. A possible evolution way of ore-forming hydrothermal fluid for the Carlin-type gold deposits in the Yunnan-Guizhou-Guangxi triangle area. *Acta Mineral Sin*. **15**, 144-149 (1995).
29. Huang, Y. *et al.* Low-temperature thermochronology of the Carlin-type gold deposits in southwestern Guizhou, China: Implications for mineralization age and geological thermal events. *Ore Geol Rev*. **115**, 103178 (2019).
30. Zhu, J. J. *et al.* No genetic link between Late Cretaceous felsic dikes and Carlin-type Au deposits in the Youjiang basin, Southwest China. *Ore Geol Rev*. **84**, 328-337 (2017).
31. Qiu, H. N. & Bai, X. J. Fluid Inclusion $^{40}$Ar/$^{39}$Ar Dating Technique and Its Applications. *Earth Sci*. **44**, 685-697 (2019).
32. Qiu, H. N. *et al.* High-precision $^{40}$Ar/$^{39}$Ar age of the gas emplacement into the Songliao Basin. *Geology*. **39**, 451-454 (2011).
33. Liu, Z. Q. *et al.* $^{40}$Ar/$^{39}$Ar geochronology constraints on hydrocarbon accumulation and destruction periods in the Bankeng paleo-reservoir in the southern margin of the middle Yangtze block. *Chinese Sci Bull*. **56**, 2803-2812 (2011).
34. Hu, R. G. *et al.* Retrograde metamorphism of the eclogite in North Qaidam, western China: Constraints by joint $^{40}$Ar/$^{39}$Ar in vacuo crushing and stepped heating. *Geosci Front*. **6**, 759–770 (2015).
35. Qiu, H. N. & Wijbrans, J. R. Paleozoic ages and excess $^{40}$Ar in garnets from the Bixiling eclogite in Dabieshan, China: New insights from $^{40}$Ar/$^{39}$Ar dating by stepwise crushing. *Geochim Cosmochim Ac*. **70**, 2354-2370 (2006).
36. Shi, K. T. *et al.* The $^{40}$Ar/$^{39}$Ar dating of quartz: new insights into the metallogenic chronology of the Jinchang gold deposit and its geological significance. *Scientific Reports*. **8**, 13879 (2018).
37. Bai, X. J. *et al.* Well-Constrained Mineralization Ages by Integrated $^{40}$Ar/$^{39}$Ar and U-Pb Dating Techniques for the Xitian W-Sn Polymetallic Deposit, South China. *Econ Geol* (2021).
38. Bai, X. J., Wang, M., Jiang, Y. D. & Qiu, H. N. Direct dating of tin-tungsten mineralization of the Piaotang Tungsten deposit, South China, by $^{40}$Ar/$^{39}$Ar progressive crushing. *Geochim Cosmochim Ac*. **114**, 1-12 (2013).
39. Jiang, Y. D., Qiu, H. N. & Xu, Y. G. Hydrothermal fluids, argon isotopes and mineralization ages of the Fankou Pb–Zn deposit in south China: Insights from sphalerite $^{40}$Ar/$^{39}$Ar progressive crushing. *Geochim Cosmochim Ac*. **84**, 369-379 (2012).
40. Turner, G. & Bannon, M. P. Argon isotope geochemistry of inclusion fluids from granite-associated mineral veins in southwest and northeast England. *Geochim Cosmochim Ac*. **56**, 227-243 (1992).
41. Xiao, M. *et al.* Gas release systematics of mineral-hosted fluid inclusions during stepwise crushing, implications for $^{40}$Ar/$^{39}$Ar geochronology of hydrothermal fluids. *Geochim Cosmochim Ac*. **251**, 36-55 (2019).
42. Kelley, S., Turner, G., Butterfield, A. W. & Shepherd, T. J. The source and significance of argon isotopes in fluid inclusions from areas of mineralization. *Earth Planet Sc Lett*. **79**, 119953 (1986).
43. Kendrick, M. A. & Phillips, D. New constraints on the release of noble gases during in vacuo crushing and application to scapolite Br-Cl-I and $^{40}$Ar/$^{39}$Ar age determinations. *Geochim Cosmochim Ac*. **73**, 5673-5692 (2009).
44. Liu, Y., Hu, K., Han, S. & Sun, Z. Structural evolution of the Youjiang Basin and its controlling effects on the formation of Carlin-type gold deposits (in Chinese). *Geological Journal of China Universities*. **21**, 1-14 (2015).
45. Jin, X. Y. *et al.* Noble gases fingerprint the source and evolution of ore-forming fluids of carlin-type gold deposits in the golden triangle, south China. *Econ Geol*. **115**, 455-469 (2020).

46. Li, Y. Q. Geology, Geochemistry and Genesis of the Liaotun Gold Depisit, Bama county, Guangxi, China. *Guilin University of Technology* (2016).
47. Hall, D. L., Sterner, S. M. & Bodnar, R. J. Freezing-Point Depression of NaCl-KCl-$H_2O$ Solutions. *Econ Geol*. **83**, 197-202 (1988).
48. Bodnar, R. J., Lecumberri-Sanchez, P., Moncada, D. & Steele-MacInnis, M. 13.5 - Fluid Inclusions in Hydrothermal Ore Deposits. *Treatise on Geochemistry (Second Edition), eds Heinrich D. Holland & Karl K. Turekian*, 119-142 (2014).
49. Shepherd, T. J. & Darbyshire, D. P. F. Fluid inclusion Rb–Sr isochrons for dating mineral deposits. *Nature*. **290**, 578-579 (1981).
50. Ni, P. *et al.* The characteristics of ore-forming fluids and mineralization mechanism in hydrothermal deposits: a case study of some typical deposits in china (in Chinese). *Bull Mineral, Petrol Geochem*. **37**, 369-394 (2018).
51. Roedder, E. Fluid inclusion analysis—Prologue and epilogue. *Geochim Cosmochim Ac*. **54**, 495-507 (1990).
52. Xiao, M., Jiang, Y.-D., Qiu, H.-N., Cai, Y. & Zhang, W.-F. An improved gas extraction model during stepwise crushing: new perspectives on fluid geochronology and geochemistry. *Ore Geol Rev*. **140**, 104588 (2022).
53. Xiao, M. *et al.* Progressively released gases from fluid inclusions reveal new insights on W-Sn mineralization of the Yaogangxian tungsten deposit, South China. *Ore Geol Rev*. **138**, 104353 (2021).
54. Bodnar, R. J. Introduction to fluid inclusions. In I. Samson, A. Anderson, & D. Marshall, eds. Fluid Inclusions: Analysis and Interpretation. Mineral. Assoc. Can., Short Course Ser. 32,31-38. (2003).
55. Bai, X.-J., Jiang, Y.-D., Hu, R.-G., Gu, X.-P. & Qiu, H.-N. Revealing mineralization and subsequent hydrothermal events: Insights from 40Ar/39Ar isochron and novel gas mixing lines of hydrothermal quartzs by progressive crushing. *Chem. Geol.* **483**, 332-341 (2018).
56. Mao, J. W., Cheng, Y. B., Mao Hong, C. & Franco, P. Major types and time–space distribution of Mesozoic ore deposits in South China and their geodynamic settings. *Miner Deposita*. **48**, 267-294 (2013).
57. Li, X. H., Bai, L. A., Yue, Z. H., Pang, B. C. & Wei, D. T. Mineralization processes involved in the formation of the Jinya Carlin-type Au deposit, northwestern Guangxi, China: Evidence from in situ trace element and S isotope geochemistry of Au-bearing zoned pyrite. *Ore Geol Rev*. **138**, 104376 (2021).
58. Bai, X.-J. *et al.* Refined insight into $^{40}Ar/^{39}Ar$ progressive crushing technique from K–Cl–Ar correlations in fluid inclusions. *Chem. Geol.* **515**, 37-49 (2019).
59. Wang, S. S. Age determinations of $^{40}Ar$-$^{40}K$, $^{40}Ar$-$^{39}Ar$ and radiogenic $^{40}Ar$ released characteristics on K-Ar geostandards of China. *Scientia Geologica Sinica*. **18**, 315-323 (1983).
60. Koppers, A. A. P. ArArCALC-software for $^{40}Ar/^{39}Ar$ age calculations. *Comput Geosci-uk*. **28**, 605-619 (2002).

# Tables

**Table 1** $^{40}Ar/^{39}Ar$ dating result for pyritization Au-bearing quartz vein from Liaotun gold deposit

| step | Pestle drop numbers | $^{36}Ar_A$ | $^{37}Ar_{Ca}$ | $^{38}Ar_{Cl}$ | $^{39}Ar_K$ | $^{40}Ar^*$ | Age ± 2σ (Ma) | $^{40}Ar^*$ (%) | $^{39}Ar_K$ (%) | K/Ca ± 2σ |
|---|---|---|---|---|---|---|---|---|---|---|
| Quartz (LT19-1-2Q) by *in vacuo* progressive crushing, $J$= 0.01985044, $I_0$=298.56 | | | | | | | | | | |
| 1 | 10 | 49.72289 | 51.0166 | 0.688294 | 272.04 | 2189.75 | 268.1±27.8 | 12.85 | 0.20 | 2.1±1.6 |
| 2 | 20 | 66.55181 | 78.8949 | 0.914396 | 559.97 | 3937.38 | 236.3±18.4 | 16.54 | 0.41 | 2.7±1.7 |
| 3 | 40 | 79.95092 | 116.2493 | 1.329468 | 1250.14 | 7878.45 | 213.1±10.0 | 24.81 | 0.92 | 4.2±2.1 |
| 4 | 60 | 65.68980 | 174.3908 | 1.571137 | 2101.32 | 11760.71 | 190.5±5.0 | 37.48 | 1.55 | 4.7±1.8 |
| 5 | 80* | 53.17219 | 163.3638 | 1.379358 | 3446.83 | 17360.23 | 172.3±2.6 | 52.22 | 2.54 | 8.2±3.0 |
| 6 | 100* | 46.14375 | 204.6715 | 1.284667 | 4426.46 | 21803.15 | 168.7±1.8 | 61.26 | 3.26 | 8.4±2.1 |
| 7 | 140* | 45.02404 | 217.0730 | 3.093739 | 6338.39 | 31498.58 | 170.1±1.3 | 70.07 | 4.67 | 11.3±4.1 |
| 8 | 180* | 41.30535 | 231.5330 | 4.032405 | 8083.37 | 40078.07 | 169.8±1.0 | 76.44 | 5.95 | 13.5±3.6 |
| 9 | 220* | 38.32218 | 217.8073 | 2.109376 | 10209.53 | 50028.87 | 167.9±0.9 | 81.36 | 7.52 | 18.1±6.6 |
| 10 | 260* | 33.71465 | 250.7197 | 1.285718 | 11277.99 | 55436.53 | 168.4±0.8 | 84.60 | 8.30 | 17.4±4.0 |
| 11 | 300* | 26.54074 | 203.8769 | 0.866962 | 12624.09 | 61663.00 | 167.3±0.7 | 88.58 | 9.29 | 24.0±5.3 |
| 12 | 350 | 23.41560 | 270.7132 | 0.769880 | 12526.18 | 64380.58 | 175.7±0.7 | 90.17 | 9.22 | 17.9±3.1 |
| 13 | 400 | 20.50324 | 218.2483 | 0.475983 | 11889.65 | 62951.96 | 180.7±0.7 | 91.10 | 8.75 | 21.1±3.0 |
| 14 | 450 | 18.49947 | 221.5877 | 0.224589 | 10158.23 | 55482.84 | 186.1±0.8 | 90.91 | 7.48 | 17.7±3.3 |
| 15 | 500 | 17.05097 | 200.5896 | 0.730391 | 8517.96 | 47935.95 | 191.5±0.8 | 90.37 | 6.27 | 16.4±4.3 |
| 16 | 550* | 14.84095 | 220.8006 | 0.232163 | 6378.95 | 37605.09 | 200.1±0.8 | 89.43 | 4.70 | 11.2±2.1 |
| 17 | 630* | 13.63239 | 186.1162 | 0.140307 | 5176.19 | 30446.97 | 199.7±0.9 | 88.18 | 3.81 | 10.8±2.5 |
| 18 | 700* | 12.62736 | 171.2247 | 0.220453 | 3891.86 | 23014.44 | 200.7±0.9 | 85.90 | 2.86 | 8.8±3.2 |
| 19 | 800* | 13.90444 | 163.7289 | 0.169922 | 3171.94 | 18843.68 | 201.6±1.0 | 81.92 | 2.33 | 7.5±2.9 |
| 20 | 800* | 11.95218 | 178.5112 | 0.200370 | 2303.52 | 13674.35 | 201.4±1.2 | 79.28 | 1.70 | 5.0±1.3 |
| 21 | 800* | 11.10584 | 158.4684 | 0.169977 | 1745.70 | 10384.65 | 201.8±1.3 | 75.78 | 1.29 | 4.3±1.4 |
| 22 | 800* | 9.29043 | 195.4351 | 0.180257 | 1434.75 | 8538.00 | 201.9±1.3 | 75.46 | 1.06 | 2.8±0.7 |
| 23 | 800* | 8.74064 | 100.6876 | 0.208530 | 1222.97 | 7237.53 | 200.9±1.4 | 73.48 | 0.90 | 4.7±2.3 |
| 24 | 800* | 8.20593 | 87.8952 | 0.237676 | 1034.93 | 6097.41 | 200.0±1.5 | 71.32 | 0.76 | 4.6±3.4 |
| 25 | 800* | 7.47681 | 75.7225 | 0.214813 | 914.01 | 5377.38 | 199.7±1.6 | 70.65 | 0.67 | 4.7±3.7 |
| 26 | 800* | 6.80959 | 65.7761 | 0.270734 | 811.30 | 4772.63 | 199.7±1.6 | 70.11 | 0.60 | 4.8±3.5 |
| 27 | 800* | 7.11494 | 84.4261 | 0.237051 | 769.97 | 4528.62 | 199.7±1.7 | 68.05 | 0.57 | 3.5±2.6 |
| 28 | 800* | 6.71301 | 59.9597 | 0.220296 | 689.95 | 4063.12 | 199.9±1.8 | 66.95 | 0.51 | 4.5±2.4 |
| 29 | 800* | 6.09843 | 68.1724 | 0.228236 | 622.25 | 3663.64 | 199.9±1.8 | 66.78 | 0.46 | 3.5±2.5 |
| 30 | 800* | 5.49046 | 60.5975 | 0.202530 | 560.52 | 3319.69 | 201.0±1.9 | 66.93 | 0.41 | 3.6±2.1 |
| 31 | 800* | 5.47876 | 72.3795 | 0.268878 | 530.42 | 3126.51 | 200.1±1.9 | 65.63 | 0.39 | 2.8±1.8 |
| 32 | 800* | 4.70585 | 75.3493 | 0.182742 | 471.27 | 2773.73 | 199.8±1.9 | 66.36 | 0.35 | 2.4±1.6 |
| 33 | 800* | 4.64396 | 51.9939 | 0.250278 | 438.76 | 2588.19 | 200.2±2.0 | 65.10 | 0.32 | 3.3±1.9 |

# Figures

### Figure 1

(a) Simplified geologic map of the tectonic framework and the location of the Golden Triangle; (b) sketch regional geological map showing the distribution of gold deposits and representative isotopic ages in and around the Golden Triangle (modified after[4]); (c) Geologic map of the Liaotun gold deposit(modified after[18]). Age references: [1]-[2]; [2]-[6]; [3]-[4]; [4]-[19]; [5]-[20]; [6]-[21]; [7]-[22]; [8]-[8]; [9]-[23]; [10]-[15]; [11]-[24]; [12]-[25]; [13]-[26]; [14]-[27]

### Figure 2

(a) Panoramic map of Liaotun gold deposit, (b) goaf of ore body IV; (c) pyritization Au-bearing quartz vein in Permian quartz sandstone Gold-bearing minerals include arsenian pyrite, arsenopyrite

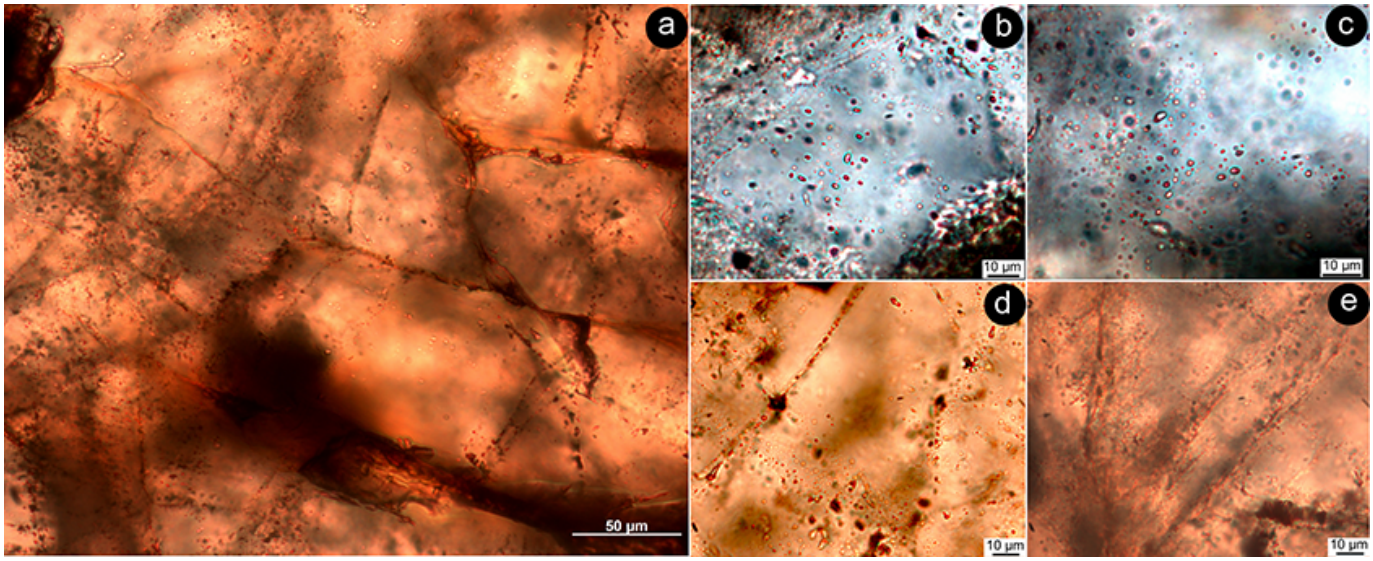


### Figure 3

Microphotographs of fluid inclusions in Au-bearing quartz vein from Liaotun gold deposit. (a) primary and secondary fluid inclusions in quartz vein; (b)–(c) isolated and clustered primary fluid inclusions in quartz vein; (d)–(e) along healed fractures and cross-cutting grain boundary secondary fluid inclusions in quartz vein

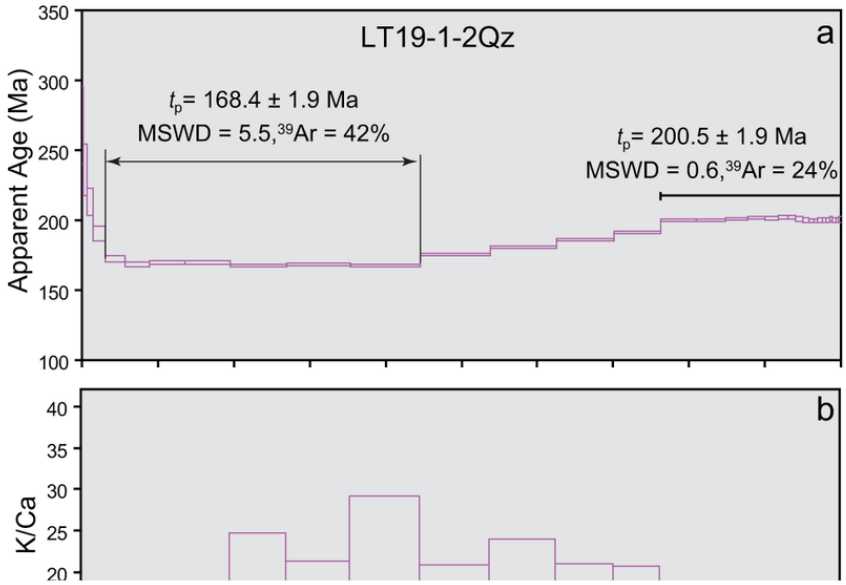


**Figure 4**

Plots based on the $^{40}Ar/^{39}Ar$ data of the quartz vein from the Liaotun Carlin-type gold deposit by *in vacuo* progressive crushing. (a) Age spectrum; (b) K/Ca spectrum; (c) inverse isochron

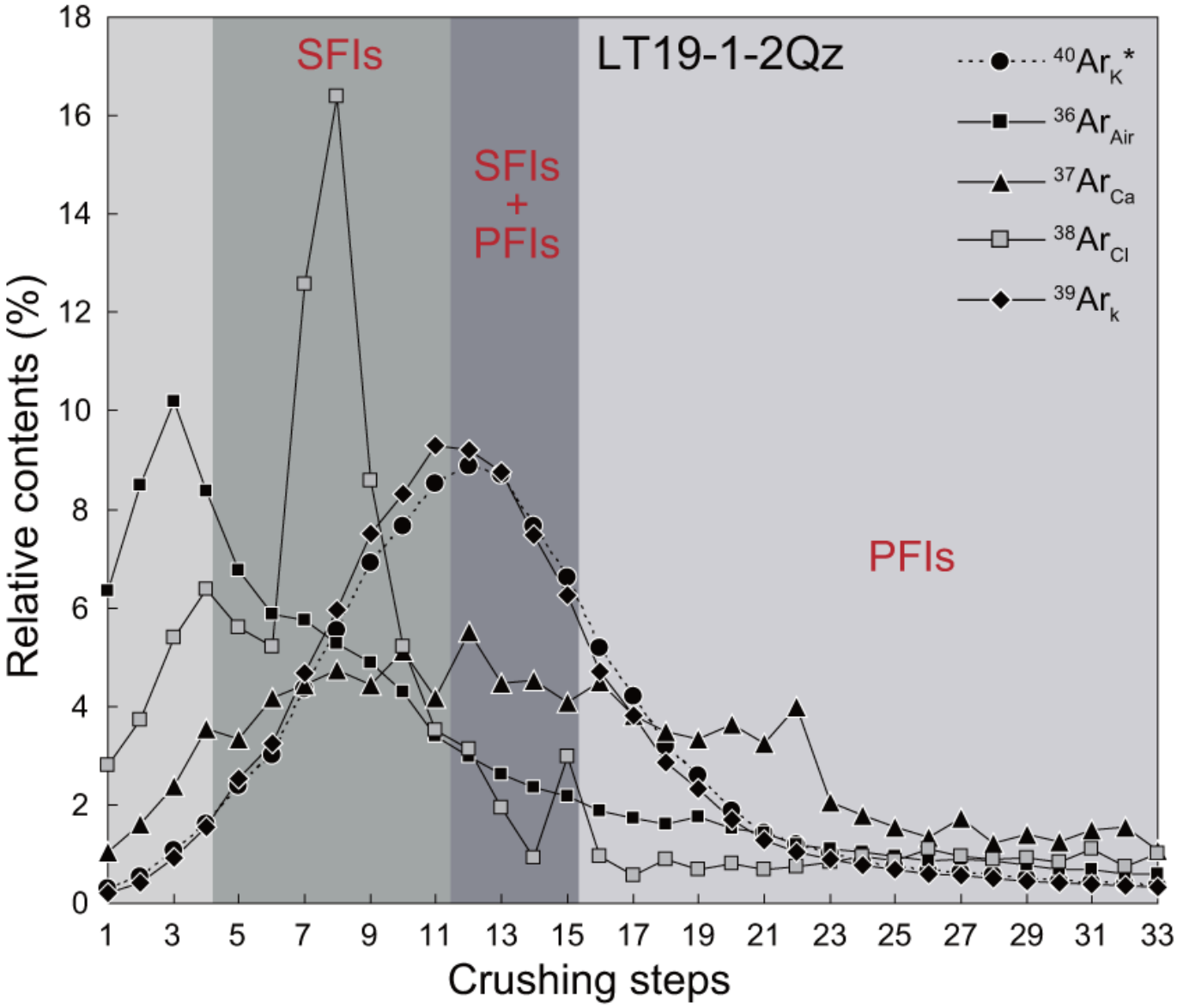


**Figure 5**

Release patterns of argon isotopes during the *in vacuo* progressive crushing experiment. All the argon isotopes are routinely applied interference corrections for the interfering nuclear reactions with isotopes of Ca, K, Ar and Cl. $^{36}Ar_{air}$–atmospheric $^{36}Ar$; $^{38}Ar_{Cl}$–produced by chlorine during irradiation after the air correction; $^{39}Ar_K$–produced in the key reaction on $^{39}K$ during irradiation; $^{40}Ar^{*}$–after air correction, including the radiogenic $^{40}Ar$ from in situ decay of $^{40}K$ and the parentless excess $^{40}Ar$.

## Supplementary Files

This is a list of supplementary files associated with this preprint. Click to download.

- SupplementaryTableS1.xls